

Anomalous Hall effect in Bernal tetralayer graphene enhanced by spin-orbit interaction

Zhuangzhuang Qu(曲壮壮), Zhihao Chen(陈志豪), Xiangyan Han(韩香岩), Zhiyu Wang(王知雨), Zhuoxian Li(李卓贤), Qianling Liu(刘倩伶), Wenjun Zhao(赵文俊), Kenji Watanabe, Takashi Taniguchi, Zhi Gang Cheng(程智刚), Zizhao Gan(甘子钊), and Jianming Lu(路建明)

Citation: Chin. Phys. B, 2025, 34 (**3**): 037201. DOI: 10.1088/1674-1056/adb411
Journal homepage: http://cpb.iphy.ac.cn; http://iopscience.iop.org/cpb

What follows is a list of articles you may be interested in

Doping tuned anomalous Hall effect in the van der Waals magnetic topological phases $Mn(Sb_{1-x}Bi_x)_4Te_7$

Xin Zhang(张鑫), Zhicheng Jiang(江志诚), Jian Yuan(袁健), Xiaofei Hou(侯骁飞), Xia Wang(王霞),Na Yu(余娜), Zhiqiang Zou(邹志强), Zhengtai Liu(刘正太), Wei Xia(夏威),Zhenhai Yu(于振海), Dawei Shen(沈大伟), and Yanfeng Guo(郭艳峰)

Chin. Phys. B, 2023, 32 (**9**): 097201. DOI: 10.1088/1674-1056/acd629

The origin of spin current in YIG/nonmagnetic metal multilayers at ferromagnetic resonance

Yun Kang(康韵), Hai Zhong(钟海), Runrun Hao(郝润润), Shujun Hu(胡树军), Shishou Kang(康仕寿), Guolei Liu(刘国磊), Yin Zhang(张引), Xiangrong Wang(王向荣), Shishen Yan(颜世申), Yong Wu(吴勇), Shuyun Yu(于淑云), Guangbing Han(韩广兵), Yong Jiang(姜勇), Liangmo Mei(梅良模)

Chin. Phys. B, 2017, 26 (**4**): 047202. DOI: 10.1088/1674-1056/26/4/047202

Spin transport in a Zigzag normal/ferromagnetic graphene junction

Shi Hao-Sheng (史豪晟), Vahram L. Grigoryan

Chin. Phys. B, 2015, 24 (**5**): 057202. DOI: 10.1088/1674-1056/24/5/057202

Localization correction to the anomalous Hall effect in amorphous CoFeB thin films

Ding Jin-Jun (丁进军), Wu Shao-Bing (吴少兵), Yang Xiao-Fei (杨晓非), Zhu Tao (朱涛)

Chin. Phys. B, 2015, 24 (**2**): 027201. DOI: 10.1088/1674-1056/24/2/027201

Spin and valley half metal induced by staggered potential and magnetization in silicene

Wang Sa-Ke (汪萨克), Tian Hong-Yu (田宏玉), Yang Yong-Hong (杨永宏), Wang Jun (汪军)

Chin. Phys. B, 2014, 23 (**1**): 017203. DOI: 10.1088/1674-1056/23/1/017203

RAPID COMMUNICATION

Anomalous Hall effect in Bernal tetralayer graphene enhanced by spin–orbit interaction

Zhuangzhuang Qu(曲壮壮)[1], Zhihao Chen(陈志豪)[2,3], Xiangyan Han(韩香岩)[1], Zhiyu Wang(王知雨)[1], Zhuoxian Li(李卓贤)[1], Qianling Liu(刘倩伶)[1], Wenjun Zhao(赵文俊)[1], Kenji Watanabe[4], Takashi Taniguchi[4], Zhi-Gang Cheng(程智刚)[2,3,†], Zizhao Gan(甘子钊)[1], and Jianming Lu(路建明)[1,‡]

[1] *State Key Laboratory for Mesoscopic Physics, School of Physics, Peking University, Beijing* 100871, *China*
[2] *Beijing National Laboratory for Condensed Matter Physics, Institute of Physics, Chinese Academy of Sciences, Beijing* 100190, *China*
[3] *University of Chinese Academy of Sciences, Beijing* 100049, *China*
[4] *National Institute for Materials Science*, 1-1 *Namiki, Tsukuba*, 305-0044, *Japan*

(Received 22 January 2025; revised manuscript received 5 February 2025; accepted manuscript online 8 February 2025)

Spin–orbit interaction (SOI) can be introduced by the proximity effect to modulate the electronic properties of graphene-based heterostructures. In this work, we stack trilayer WSe_2 on Bernal tetralayer graphene to investigate the influence of SOI on the anomalous Hall effect (AHE). In this structurally asymmetric device, by comparing the magnitude of AHE at positive and negative displacement fields, we find that AHE is strongly enhanced by bringing electrons in proximity to the WSe_2 layer. Meanwhile, the enhanced AHE signal persists up to 80 K, providing important routes for topological device applications at high temperatures.

Keywords: anomalous Hall effect, proximity effect, Bernal tetralayer graphene, spin–orbit interaction

PACS: 72.80.Vp, 73.40.–c

DOI: 10.1088/1674-1056/adb411 **CSTR:** 32038.14.CPB.adb411

1. Introduction

Intrinsic anomalous Hall effect (AHE) in graphene systems relies on the breaking of valley symmetry, which brings in finite Berry curvature in the momentum space. While a pristine graphene itself has spin-and-valley four-fold degeneracies, strong electronic interaction or spin–orbit interaction (SOI) has been routinely utilized to break the valley symmetry. For the electronic interaction, it can be brought in by flatting the band dispersion via twist engineering[1,2] and/or applying perpendicular displacement fields (D) in a rhombohedral/Bernal multilayer graphene.[3–9] For the latter, proximity to transition metal dichalcogenides (TMDs), whose SOI is in the order of 100 meV, effectively induces SOI into graphene, leading to weak antilocalization[10–19] and (quantized) anomalous Hall effect.[20–22] In rhombohedral trilayer/tetralayer graphene, both electronic interaction and SOI have been applied to observe the enhancement of critical temperature and the topological nature of superconductivity.[23–25]

As a highly tunable quantum platform, Bernal tetralayer graphene (BTG) has been widely studied.[26–33] In particular, AHE was found in BTG and surprisingly survived up to 70 K, which was ascribed to spontaneous breaking of the valley degeneracy.[9] It would be interesting to examine whether the phenomenon can survive above liquid nitrogen temperature by further involving SOI. In this work, trilayer WSe_2 is placed under the bottom surface of BTG to introduce SOI. We find that the magnitude of AHE in BTG is greatly enhanced by bringing electrons closer to the WSe_2 layer via a negative D. The asymmetric dependence of AHE on positive and negative D directly proves the important role of SOI in observing AHE. Naturally, the critical temperature of this enhanced AHE can be increased to 80 K.

2. Methods

Figure 1(a) shows the optical image and measurement schematic of the device. The number of layers is distinguished by optical contrast[34] and the stacking order of the tetralayer graphene is identified by Raman spectroscopy.[35] The thicknesses of top and bottom hBN are 22 nm and 16 nm, respectively. Trilayer rather than monolayer WSe_2 is chosen, because it is more mechanically robust during manual stacking and easier to obtain through mechanical exfoliation. Note that the thickness of WSe_2 is not an important parameter to introduce SOI into graphene.[20,36–38] The twist angle between WSe_2 and graphene is around 15°. The device is fabricated via the standard dry transfer methods.[39,40] Thick graphite layers are used as top and bottom gate electrodes to control the carrier concentration $n = (C_{bg}V_{bg} + C_{tg}V_{tg})/e$ and the displacement field $D = (C_{bg}V_{bg} - C_{tg}V_{tg})/2\varepsilon_0$. Here, $C_{tg(bg)}$, $V_{tg(bg)}$, e, ε_0 donate top (bottom) geometric capacitance, top (bottom) gate voltages, elementary charge, vacuum permittivity, respectively. The resistance is measured in the Oxford Teslatron system using standard lock-in techniques.

†Corresponding author. E-mail: zgcheng@iphy.ac.cn
‡Corresponding author. E-mail: jmlu@pku.edu.cn

© 2025 Chinese Physical Society and IOP Publishing Ltd. All rights, including for text and data mining, AI training, and similar technologies, are reserved.

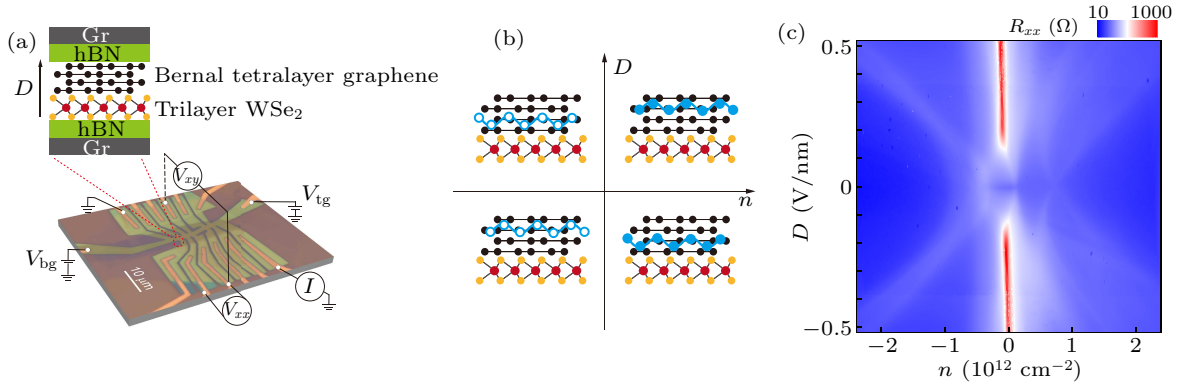


Fig. 1. (a) Device schematic and measurement configuration. Scale bar: 10 μm. In the cross section, a Bernal tetralayer graphene is stacked on a trilayer WSe_2, which are further encapsulated by hBN (green) and graphite gates (grey). (b) Spatial distribution of charge carriers schematically plotted in the D–n diagram, where the blue wavy line illustrates the wave function and blue filled circles (blue empty circles) represent electrons (holes). (c) Longitudinal resistance R_{xx} as a function of carrier density (n) and displacement field (D) at 300 mK.

3. Results and analysis

Depending on the device structure and the defined direction of displacement field in Fig. 1(a), the carrier distribution of conduction (valence) band in the D–n diagram is schematically shown in Fig. 1(b). For an ideal layer-polarization system like Bernal bilayer graphene or rhombohedral multilayer graphene, under a positive displacement field, electrons will have a lower potential energy at the bottom surface, thus the valence band is locked with the bottom surface and the conduction band is locked with the top surface. General speaking, the low-energy band structure of BTG can be considered as two sets of bilayer graphene-like bands with interaction.[26] In BTG, layer polarization is far from being ideal, nevertheless, we can still draw a similar conclusion about the relationship between the spatial distribution of carriers and the displacement field. In our asymmetric device, as electrons (holes) approach WSe_2 in the case of a negative (positive) D and a positive (negative) n (Fig. 1(b)), the proximity effect becomes more pronounced and we expect to gain a substantial SOI in BTG. Figure 1(c) shows the longitudinal resistance R_{xx} map diagram at 300 mK, where a resistance minimum at the charge neutrality point with $D = 0$ and tunable multi-resistance peaks associated with Lifshitz transitions are clearly observed. These remarkable features are consistent with the previously reported transport characteristics of BTG, indicating the high quality of our device.[9,29]

In order to systematically explore the influence of SOI on AHE, we select some points with the same n and opposite D on the electron side, where the AHE signal has been observed to be more pronounced than that on the hole side,[9] to obtain Hall resistance R_{xy}. By using the formula[41] $R_{xy}(B) = \eta B + R_{\rm AH}$, $\eta = 1/(ne)$, where η is the linear Hall coefficient, and $R_{\rm AH}$ is the anomalous Hall resistance, R_{xy} is decomposed into a linear part and an anomalous part. The extracted $R_{\rm AH}$ at different points (n, D) are shown in Fig. 2. Overall, $R_{\rm AH}$ increases and then saturates at ~ 0.03 T. We denote the difference between the saturated $R_{\rm AH}$ plateaus formed in positive and negative magnetic fields as $\Delta R_{\rm AH}$ to characterize the intensity of the AHE (Fig. 2(b)). It shows a significant dependence on the signs of displacement field: $\Delta R_{\rm AH}(-D) > \Delta R_{\rm AH}(+D)$. As shown in the inset of Fig. 2(a), when $D > 0$ for which electrons are farther away from WSe_2, a weakened AHE is observed. In contrast, when $D < 0$, electrons are closer to WSe_2 and the AHE is enhanced.

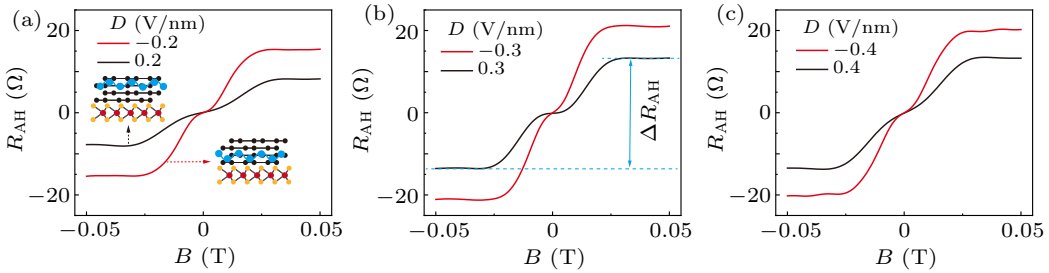


Fig. 2. Anomalous Hall resistance $R_{\rm AH}$ at $n = 0.2 \times 10^{12}$ cm^{-2} as a function of magnetic field at ± 0.2 V/nm (a), ± 0.3 V/nm (b), ± 0.4 V/nm (c). The black (red) line represents $+D$ ($-D$). Inset of (a): Schematic distribution of carriers (blue wave). Inset of (b): Definition of $\Delta R_{\rm AH}$.

The enhancement of AHE by pushing carriers in proximity to WSe_2 is found to be effective over a large range of carrier density. In Fig. 3, we fix D and change n to examine the variance of $R_{\rm AH}$. Both at $D = \pm 0.3$ V/nm and ± 0.4 V/nm, $\Delta R_{\rm AH}$ becomes smaller with the increasing n, indicating that AHE is more significant in the low carrier region.[9] This is reasonable, since the symmetry breaking of spin and valley degrees is most significant at low carrier densities.[3,8] The increase of

n weakens the symmetry-breaking effect, and then the Berry curvature is washed out, so is AHE. For electrons moves away from WSe_2 under a positive D, ΔR_{AH} decays quickly. However, when D is negative, significant SOI is introduced into BTG, resulting in considerable ΔR_{AH} even in the high carrier region (Figs. 3(c) and 3(f)). In brief, SOI expands the significant AHE to a larger carrier density.

Besides the extended carrier range, the working temperature of AHE is observed to be significantly enhanced. Here, we select the two typical points ($D = \pm 0.4$ V/nm and $n = 0.05 \times 10^{12}$ cm^{-2}) which exhibit the largest ΔR_{AH} at 300 mK, and conduct the variable-temperature Hall resistance measurement (Fig. 4). At all temperatures, we find that $\Delta R_{AH}(-D) > \Delta R_{AH}(+D)$, which, again, confirms the influence of the introduced SOI on AHE. As temperature rises, thermal fluctuation suppresses the electron–electron interaction, leading to a weakened symmetry breaking effect that ultimately destroys AHE. The introduction of SOI counteracts this negative effect of temperature. In Fig. 4(i), the enhanced ΔR_{AH} can still be observed at 80 K, higher than liquid nitrogen temperature and the reported 70 K in the literatures.[9] This is of great significance for the application of AHE in high temperature quantum devices.[1–3,21,22]

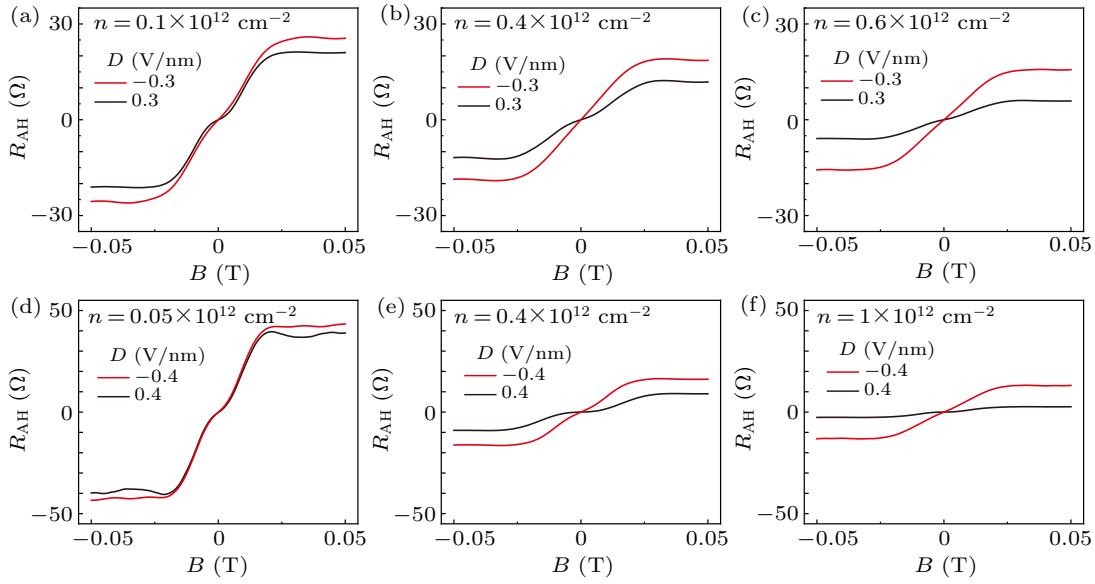


Fig. 3. AHE with different n. (a)–(c) R_{AH} at $D = \pm 0.3$ V/nm with $n = 0.1 \times 10^{12}$ cm^{-2} (a), 0.4×10^{12} cm^{-2} (b) and 0.6×10^{12} cm^{-2} (c). (d)–(f) R_{AH} at $D = \pm 0.4$ V/nm with $n = 0.05 \times 10^{12}$ cm^{-2} (d), 0.4×10^{12} cm^{-2} (e) and 1×10^{12} cm^{-2} (f).

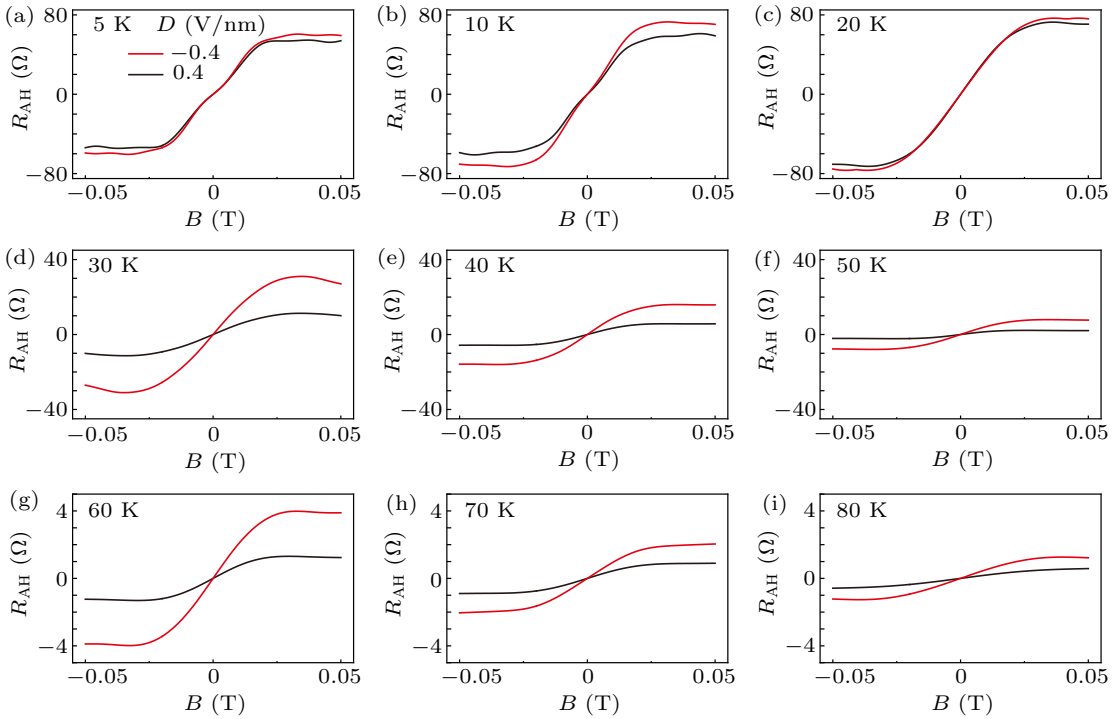


Fig. 4. The temperature dependence of AHE at $D = \pm 0.4$ V/nm and $n = 0.05 \times 10^{12}$ cm^{-2}, including 5 K (a), 10 K (b), 20 K (c), 30 K (d), 40 K (e), 50 K (f), 60 K (g), 70 K (h) and 80 K (i). The solid red (black) line represents $D = -0.4$ (+0.4) V/nm.

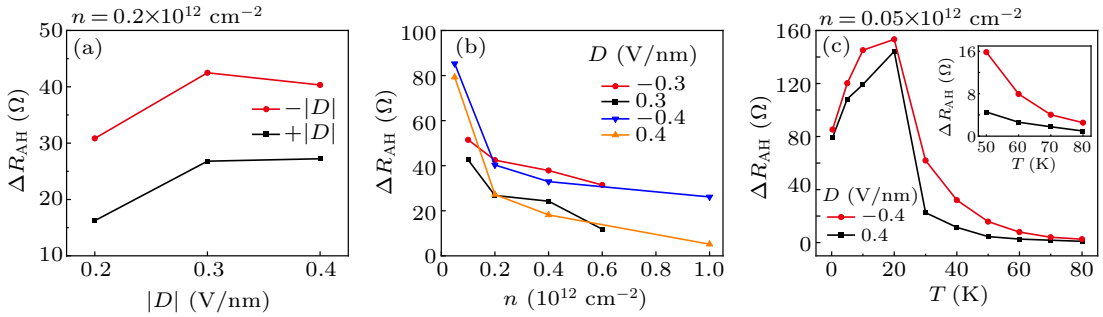


Fig. 5. (a) $\Delta R_{\rm AH}$ at $n = 0.2 \times 10^{12}$ cm^{-2} as a function of $|D|$. (b) $\Delta R_{\rm AH}$ at $D = \pm 0.3$ V/nm and ± 0.4 V/nm with different n. (c) The temperature dependence of $\Delta R_{\rm AH}$ at $D = \pm 0.4$ V/nm and $n = 0.05 \times 10^{12}$ cm^{-2}. Inset: An enlarged view at high temperatures.

In the end, we summarize the enhancement of $\Delta R_{\rm AH}$ as a function of displacement field (Fig. 5(a)), carrier density (Fig. 5(b)) and temperature (Fig. 5(c)). As can be seen, the introduced SOI does not change the original dependences of AHE on various physical parameters: it would also be enhanced by a large D, but suppressed by a large n, and a non-monotonic relationship with temperature, which are consistent with previous observation.[9] However, the magnitude of AHE is universally promoted, regardless the varied physical parameters.

4. Conclusion

In this work, we fabricate high-quality Bernal tetralayer graphene–trilayer WSe_2 device to investigate the influence of spin–orbit coupling on anomalous Hall effect. Given that the WSe_2 layer rests on one side of the tetralayer graphene, the structural asymmetry renders the AHE highly sensitive to the positive and negative signs of displacement field. Specifically, AHE intensifies when the carriers approach the WSe_2 layer and is weakened otherwise. Furthermore, the enhanced AHE persists to a large range of carrier density and, more importantly, a working temperature up to 80 K, offering a promising route for achieving high-temperature topological devices.

Acknowledgements

Project supported by the National Key R&D Program of China (Grant Nos. 2021YFA1400100 and 2024YFA1409700) and the National Natural Science Foudation of China (Grant Nos. 12374168 and T2325026).

References

[1] Sharpe A L, Fox E J, Barnard A W, Finney J, Watanabe K, Taniguchi T, Kastner M A and Goldhaber-Gordon D 2019 *Science* **365** 605
[2] Serlin M, Tschirhart C L, Polshyn H, Zhang Y, Zhu J, Watanabe K, Taniguchi T, Balents L and Young A F 2020 *Science* **367** 900
[3] Zhou H, Xie T, Ghazaryan A, Holder T, Ehrets J R, Spanton E M, Taniguchi T, Watanabe K, Berg E, Serbyn M and Young A F 2021 *Nature* **598** 429
[4] Liu K, Zheng J, Sha Y, Lyu B, Li F, Park Y, Ren Y, Watanabe K, Taniguchi T, Jia J, Luo W, Shi Z, Jung J and Chen G 2024 *Nat. Nanotechnol.* **19** 188
[5] Han T, Lu Z, Scuri G, Sung J, Wang J, Han T, Watanabe K, Taniguchi T, Fu L, Park H and Ju L 2023 *Nature* **623** 41
[6] Han T, Lu Z, Scuri G, Sung J, Wang J, Han T, Watanabe K, Taniguchi T, Park H and Ju L 2024 *Nat. Nanotechnol.* **19** 181
[7] Zhou H, Holleis L, Saito Y, Cohen L, Huynh W, Patterson C L, Yang F, Taniguchi T, Watanabe K and Young A F 2022 *Science* **375** 774
[8] Seiler A M, Geisenhof F R, Winterer F, Watanabe K, Taniguchi T, Xu T, Zhang F and Weitz R T 2022 *Nature* **608** 298
[9] Chen H, Arora A, Song J C W and Loh K P 2023 *Nat. Commun.* **14** 7925
[10] Wang Z, Ki D, Chen H, Berger H, MacDonald A H and Morpurgo A F 2015 *Nat. Commun.* **6** 8339
[11] Yang B, Tu M F, Kim J, Wu Y, Wang H, Alicea J, Wu R, Bockrath M and Shi J 2016 *2D Mater.* **3** 031012
[12] Wang Z, Ki D K, Khoo J Y, Mauro D, Berger H, Levitov L S and Morpurgo A F 2016 *Phys. Rev. X* **6** 041020
[13] Yang B, Lohmann M, Barroso D, Liao I, Lin Z, Liu Y, Bartels L, Watanabe K, Taniguchi T and Shi J 2017 *Phys. Rev. B* **96** 041409
[14] Völkl T, Rockinger T, Drienovsky M, Watanabe K, Taniguchi T, Weiss D and Eroms J 2017 *Phys. Rev. B* **96** 125405
[15] Wakamura T, Reale F, Palczynski P, Guéron S, Mattevi C and Bouchiat H 2018 *Phys. Rev. Lett.* **120** 106802
[16] Wakamura T, Reale F, Palczynski P, Zhao M Q, Johnson A T C, Guéron S, Mattevi C, Ouerghi A and Bouchiat H 2019 *Phys. Rev. B* **99** 245402
[17] Tiwari P, Srivastav S K and Bid A 2021 *Phys. Rev. Lett.* **126** 096801
[18] Fülöp B, Márffy A, Zihlmann S, Gmitra M, Tóvári E, Szentpéteri B, Kedves M, Watanabe K, Taniguchi T, Fabian J, Schönenberger C, Makk P and Csonka S 2021 *npj 2D Mater. Appl.* **5** 82
[19] Amann J, Völkl T, Rockinger T, Kochan D, Watanabe K, Taniguchi T, Fabian J, Weiss D and Eroms J 2022 *Phys. Rev. B* **105** 115425
[20] Lin J X, Zhang Y H, Morissette E, Wang Z, Liu S, Rhodes D, Watanabe K, Taniguchi T, Hone J and Li J I A 2022 *Science* **375** 437
[21] Sha Y, Zheng J, Liu K, Du H, Watanabe K, Taniguchi T, Jia J, Shi Z, Zhong R and Chen G 2024 *Science* **384** 414
[22] Han T, Lu Z, Yao Y, Yang J, Seo J, Yoon C, Watanabe K, Taniguchi T, Fu L, Zhang F and Ju L 2024 *Science* **384** 647
[23] Patterson C L, Sheekey O I, Arp T B, Holleis L F W, Koh J M, Choi Y, Xie T, Xu S, Redekop E, Babikyan G, Zhou H, Cheng X, Taniguchi T, Watanabe K, Jin C, Lantagne-Hurtubise E, Alicea J and Young A F 2024 arXiv:2408.10190 [cond-mat.mes-hall]
[24] Yang J, Shi X, Ye S, Yoon C, Lu Z, Kakani V, Seo J, Shi L, Watanabe K, Taniguchi T, Zhang F and Ju L 2024 arXiv:2408.09906 [cond-mat.supr-con]
[25] Han T, Lu Z, Yao Y, Shi L, Yang J, Seo J, Ye S, Wu Z, Zhou M, Liu H, Shi G, Hua Z, Watanabe K, Taniguchi T, Xiong P, Fu L and Ju L 2024 arXiv:2408.15233 [cond-mat.mes-hall]
[26] Koshino M and McCann E 2011 *Phys. Rev. B* **83** 165443
[27] Grushina A L, Ki D K, Koshino M, Nicolet A A L, Faugeras C, McCann E, Potemski M and Morpurgo A F 2015 *Nat. Commun.* **6** 6419
[28] Wu Z, Han Y, Lin J, Zhu W, He M, Xu S, Chen X, Lu H, Ye W, Han T, Wu Y, Long G, Shen J, Huang R, Wang L, He Y, Cai Y, Lortz R, Su D and Wang N 2015 *Phys. Rev. B* **92** 075408
[29] Shi Y, Che S, Zhou K, Ge S, Pi Z, Espiritu T, Taniguchi T, Watanabe K, Barlas Y, Lake R and Lau C N 2018 *Phys. Rev. Lett.* **120** 096802
[30] Hirahara T, Ebisuoka R, Oka T, Nakasuga T, Tajima S, Watanabe K, Taniguchi T and Yagi R 2018 *Sci. Rep.* **8** 13992
[31] Che S, Shi Y, Yang J, Tian H, Chen R, Taniguchi T, Watanabe K, Smirnov D, Lau C N, Shimshoni E, Murthy G and Fertig H A 2020 *Phys. Rev. Lett.* **125** 036803

[32] Liang M, Li S and Gao J H 2022 *Phys. Rev. B* **105** 045419
[33] Klanurak I, Watanabe K, Taniguchi T, Chatraphorn S and Taychatanapat T 2024 *Nano Lett.* **24** 6330
[34] Bing D, Wang Y, Bai J, Du R, Wu G and Liu L 2018 *Opt. Commun.* **406** 128
[35] Cong C, Yu T, Sato K, Shang J, Saito R, Dresselhaus G F and Dresselhaus M S 2011 *ACS Nano* **5** 8760
[36] Avsar A, Tan J Y, Taychatanapat T, Balakrishnan J, Koon G K W, Yeo Y, Lahiri J, Carvalho A, Rodin A S, O'Farrell E C T, Eda G, Castro Neto A H and Özyilmaz B 2014 *Nat. Commun.* **5** 4875
[37] Siriviboon P, Lin J X, Scammell H D, Liu S, Rhodes D, Watanabe K, Taniguchi T, Hone J, Scheurer M S and Li J I A 2021 arXiv:2112.07127v1 [cond-mat.mes-hall]
[38] Lin J X, Siriviboon P, Scammell H D, Liu S, Rhodes D, Watanabe K, Taniguchi T, Hone J, Scheurer M S and Li J I A 2022 *Nat. Phys.* **18** 1221
[39] Kim K, Yankowitz M, Fallahazad B, Kang S, Movva H C P, Huang S, Larentis S, Corbet C M, Taniguchi T, Watanabe K, Banerjee S K, LeRoy B J and Tutuc E 2016 *Nano Lett.* **16** 1989
[40] Iwasaki T, Endo K, Watanabe E, Tsuya D, Morita Y, Nakaharai S, Noguchi Y, Wakayama Y, Watanabe K, Taniguchi T and Moriyama S 2020 *ACS Appl. Mater. Interfaces* **12** 8533
[41] Nagaosa N, Sinova J, Onoda S, MacDonald A H and Ong N P 2010 *Rev. Mod. Phys.* **82** 1539